JOURNAL OF GEOPHYSICAL RESEARCH, VOL. 87, NO. B5, PAGES 3873–3884, MAY 10, 1982

Frequency Characteristics of Acoustic Emission in Rocks Under Uniaxial Compression and Its Relation to the Fracturing Process to Failure

MITIYASU OHNAKA AND KIYOO MOGI

Earthquake Research Institute, University of Tokyo, Bunkyo-ku, Tokyo 113, Japan

Acoustic emissions generated during the uniaxial compression of brittle rocks were counted after band-pass filtering. Throughout the whole process from application of load to failure, the count rate monitored through a low pass window was compared statistically with that monitored through a high pass window. The emission rate monitored through a low pass window increases more rapidly than that monitored through a high pass window as rock approaches failure. Two possible explanations for this effect are (1) generation of larger cracks (or coalescence of cracks into larger sizes) and (2) the relative attenuation of higher-frequency wave components. This finding is consistent with past observations, i.e., the relative number of large-amplitude events increases (i.e., a decrease in *b* value) as rock approaches failure. We suggest that larger cracks tend to generate events with larger amplitudes and containing lower-frequency components. The frequency characteristics of acoustic emissions are used to characterize the microfracturing processes leading to failure. The beginning of a sequence of acoustic emission activity is discussed in relation to the stress-strain curve and the onset of dilatancy. The present observations may be utilized in understanding structural instability of a region where rockbursts or earthquakes can potentially occur. If a sizable microseismic population is observed through sensors placed near the fault, then a potential exists for predicting major earthquakes.

INTRODUCTION

When rock in brittle regime is stressed to failure, microcracking occurs prior to macroscopic fracture. To understand the microcracking processes leading to failure, authors have studied (1) volumetric strain [*Brace et al.*, 1966], electrical resistivity [*Brace and Orange*, 1968], or elastic wave velocity [e.g., *Matsushima*, 1960; *Nur and Simmons*, 1969] measurements made under stress, from which some averaged property of dilatant cracking is inferred, (2) the shape and location of individual cracks and pores with a scanning electron microscope [*Sprunt and Brace*, 1974; *Tapponnier and Brace*, 1976; *Kranz*, 1979*a*, *b*], and (3) acoustic emission [e.g., *Obert and Duval*, 1942; *Mogi*, 1962*a*, 1968; *Scholz*, [1968*a*, *d*; *Byerlee and Lockner*, 1977; *Lockner and Byerlee*, 1977*a*, *b*; *Sondergeld and Estey*, 1981; *Nishizawa et al.*, 1981]. The present paper is primarily concerned with acoustic emissions generated by cracking.

There are several approaches to studying acoustic emissions, for example (1) observation of the emission activity by counting the event rate (or the cumulative numbers), (2) determination of the source locations, (3) examination of the amplitude distributions, (4) investigation on frequency characteristics of emission events, and (5) study of the source mechanism for individual emission events. Each of these studies can provide important information concerning various aspects of the fracturing processes. For instance, observation of the emission activity [e.g., *Obert and Duval*, 1942; *Mogi*, 1962*a*; *Scholz*, 1968*a*] and examination of the amplitude distributions [e.g., *Mogi*, 1962*b*, 1981; *Scholz*, 1968*d*] make it possible to monitor instability of brittle rock, and determination of the source locations [e.g., *Scholz*, 1968*b*; *Mogi*, 1968; *Byerlee and Lockner*, 1977; *Lockner and Byerlee*, 1977*a*, *b*; *Sondergeld and Estey*, 1981; *Nishizawa et al.*, 1981] enables one to monitor the location of failure zones.

Study of the frequency characteristics of emission events, on which our attention will be focussed, could be significant and promising as a means of characterzing the fracturing processes leading to failure. Numerous studies have been conducted on this subject [*Shamina*, 1956; *Chugh et al.*, 1972; *Kanagawa et al.*, 1977; *Kusunose et al.*, 1980]. In most earlier studies, attention was paid to the change in spectral amplitudes of emission events over a wide bandwidth of monitoring frequencies with increasing applied stress, and conflicting results have been reported. Many difficulties are involved in the study of frequency spectra of individual acoustic emission events [e.g., *Hardy*, 1972]. Frequency characteristics of the monitoring system (including the sensor itself) are very important in investigating this subject; however, few authors have included a detailed description of the systems used. A statistical approach is indispensable when the spectra of individual acoustic emissions generated in different stages of the fracturing processes are compared because emission events, even if they are generated during a short time interval in the same stage, differ from one another in the waveform (or the frequency content) and because a large number of such events generated during a short time interval (say, several tens or more per second) make it impossible to examine the spectra of all these events [*Ohnaka and Mogi*, 1981]. Such a statitical approach has been overlooked in spite of its importance in most of the earlier studies. For the reasons stated above, the earlier results should be considered with caution.

The purpose of this paper is first to present data on the (spectral) frequency dependence of acoustic emission activity during the microcracking processes leading up to failure and then to discuss the microcracking process itself on the basis of the results obtained in the experiments. It has been reported [e.g., *Scholz*, 1968*a*] that the beginning of a sequence of acoustic emission activity corresponds to the

Paper number 2B0137.
0148-0227/82/002B-0137$05.00

TABLE 1. Transducers Used

Monitoring Channel (Frequency Window)	PZT Disk: Size, mm	PZT Disk: Nominal Rezonance Frequency	Transducer Size, mm	Remarks
L	$10^{\phi} \times 2$	f_{33} = 1 MHz f_p = 200 kHz	$13^{\phi} \times 16$	commercially available accelerometer; natural frequency = 140 kHz; contact resonance frequency = ~30 kHz
I_1	$10^{\phi} \times 2$	f_{33} = 1 MHz f_p = 200 kHz	$14^{\phi} \times 8$	homemade sensor
I_2	$5^{\phi} \times 1$	f_{33} = 2 MHz f_p = 400 kHz	$9^{\phi} \times 7$	homemade sensor
H	$5^{\phi} \times 1$	f_{33} = 2 MHz f_p = 400 kHz	$9^{\phi} \times 7$	homemade sensor; higher mode $3f_p$ accentuated

f_{33}, resonant frequency in the thickness direction, and f_p, resonant frequency in the radius direction.

onset of dilatancy defined as the beginning of the nonlinear part of the axial stress-volumetric strain curve above about half the failure strength. However, it will be shown in this paper that a sequence of acoustic emission activity in rock begins prior to the onset of appreciable dilatancy. The method of approach taken in our experiments is outlined in a previous paper [*Ohnaka and Mogi,* 1981].

EXPERIMENTAL METHOD

The lead zirconate titanate disks polarized in the thickness direction each shielded by a metal case were used as the receiving transducers (Table 1). The piezoelectric constants (g_{33} = 31.2 × 10^{-3} V m/N and g_{31} = 9.5×10^{-3} V m/N) and the electromechanical coupling factors (k_{33} = 0.75 and k_p = 0.65) for the ceramic disks used are of the same order of magnitudes in the plane perpendicular to the polarization direction (i.e., thickness direction) as in the polarization direction itself. These piezoelectric transducers have sensitivity peaks at the frequencies resonant to each dimension of both thickness and diameter of the ceramic disks and to the dimensions of the transducer case, and their higher modes will also appear. Furthermore, when the transducer is attached to a specimen, the contact resonance [*Furukawa,* 1966] will appear due to the local stiffness in the region of attachment. Hence, the transducers cannot have a flat frequency response over a wideband of frequencies: They have multiple sensitivity peaks [*Ohnaka and Mogi,* 1981]. Some of these peaks were accentuated through the use of active band-pass filters to create narrow bandwidth windows through which acoustic emissions were monitored, as will be described below. We compare the count rate of the emission events monitored through a low-frequency window with that simultaneously recorded through a higher-frequency window throughout an experiment. In this approach, all of the emission events counted simultaneously during each experiment through two different frequency windows are compared statistically.

The output of each transducer was preamplified and filtered before being inserted into the main amplifier and the secondary filter (see Table 2), and the resulting signals were fed into an electronic circuitry which may be called discriminator, designed for assuring one pulse for one acoustic emission event by selecting both a threshold level of a comparator and a dead time of a gate. The pulses from the discriminator were counted (by an electronic counter), converted to the analog signals, and recorded by a strip chart recorder to monitor the count rate of acoustic emission events during a test. In the present experiments the acoustic emission rate was sampled every 10 s for the duration of the tests. A dual-beam oscilloscope was used to check the operation of the system and to monitor the acoustic emission signals.

Four different narrow frequency bands were selected for the present study (cf. Table 2 and Figure 1); a low-frequency window L (with sensitivity peaks around 30 kHz), two intermediate frequency windows I_1 (~250 kHz) and I_2 (250 kHz ~ 400 kHz), and a high-frequency window H (~1 MHz). Figure 1 shows frequency response of the overall monitoring channel (including the sensor itself) for each frequency window selected above. As stated above, a piezoelectric transducer has multiple sensitivity peaks (and multiple 'dead bands'), and hence the transducer itself is a kind of

TABLE 2. Monitoring System Used

Monitoring Channel (Frequency Window)	Amplifier Gain (Pre + Main), dB	Filter (1 + 2) Band Pass†	Noise Level of Overall Monitoring Channel including Sensor‡, μV
L	86	20–400 kHz	12
I_1	66	100–300 kHz	7
I_2	86*	300–400 kHz	5
H	86	1–1.5 MHz	5

*Effective gain 78 dB at 250 kHz.

†Since a piezoelectric transducer itself is a kind of filter, note that net width of the passband is narrower than the filter bandwidth.

‡Voltage peak amplitude referred to input. The noise level differs between the monitoring channels due to the difference in the sensor's noise level.

filter. Thus note that net width of the pass band for each frequency window is narrower than the filter bandwidth. The frequency responses shown in Figure 1 were obtained by using nominally identical transducers (kept in contact with the two opposite faces of a brass disk with nearly equal dimensions to the adapters used) for both transmitting and receiving a sinusoidal wave over a wide range of frequencies and by adjusting the gain of the amplifiers so as to have nearly the same sensitivity peaks between the monitoring channels for the four different frequency windows selected. Since only two channels of the monitoring facilities were available for this study, two frequency windows such as (L, I_2) and (I_1, H) were chosen out of the four for an experiment, and acoustic emissions were monitored and counted simultaneously through the two different frequency windows throughout each experiment.

We notice from Figure 1 that there are multiple narrow 'dead bands' of the sensitivity. These 'dead bands' may be ascribed to the effect of the brass disk put between the transmitting and receiving transducers. In general, since an emission event is a rapid physical change in a material and acoustic emission is basically pulse transient in nature, the emission waves contain a relatively broad spectrum of frequencies. If this spectrum is broader than the maximum of the widths of these 'dead bands,' then event counts are not influenced by the existence of such narrow 'dead bands.' We believe that the spectrum of an emission event is in general broader than the maximum of the widths of those 'dead bands.' An important point in our approach is that the overall frequency response of the monitoring system (including the sensor itself) for each frequency window is unchanged during an experiment and that the rates of the emission events counted simultaneously through different frequency windows can easily be compared statistically throughout the experiment.

The duration time of an acoustic emission varies according to a frequency window through which it is observed (see Figure 2). Suitable values of the dead time were determined for each frequency window; about 2 ms for the low-frequency window L, about 0.5 ms for the intermediate frequency windows I_1 and I_2, and about 0.04 ms for the high-frequency window H [*Ohnaka and Mogi*, 1981]. When the duration of an acoustic emission exceeds the dead time interval T set for each frequency window, the dead time length is automatically prolonged by another time interval T in our counting system. The threshold level of each channel was balanced above the noise level before each experiment so as to keep the count rates from the two different channels significant and comparable. Our high sensitivity and low noise counting system (Table 2) could detect acoustic events having voltage peak amplitudes less than 15 μV referred to input. However, if all of these very small events above the noise level are considered, then some bursts of emission observed may be composed of several emission events occurring within the same time interval. This will make it impossible to assure one pulse for one emission event. To avoid such a situation, it is intended in this study that only the emission events exceeding a certain, relatively high level of threshold far above the noise level be monitored and counted. It is true that the count level depends upon the sensitivity and the threshold level set for each channel. But they were fixed throughout an experiment.

Two rocks, Shinkomatsu andesite (SAN) and Mannari granite (MGR), were used in this study (Table 3). The shape of the specimens was a right circular cylinder, 12.5 cm long and 5 cm in diameter. All were cored in the same direction from a single block for each rock. The ends were ground parallel to ±0.0003 cm/cm. Steel end caps and epoxy fillets were affixed to the ends of the specimens in a manner similar to that described by *Mogi* [1966] to reduce end effects. Earlier studies [*Scholz*, 1968*b*; *Lockner and Byerlee*, 1977*a*, *b*; *Sondergeld and Estey*, 1981; *Nishizawa et al.*, 1981; S. Yoshikawa, personal communication, 1981] showed that most of the emission events generated during compression are distributed over the middle part of the specimen rather than near the ends, as would be expected if stress concentrations owing to end effects were important. Four electric resistance strain gages (effective grid sizes 20 × 5 mm) were cemented directly at the middle of the sample side surface, both parallel (two gages, diametrically opposite to each other) and perpendicular (two gages, diametrically opposite to each other) to the cylinder axis. This allows one to calculate the volumetric strain.

The two receiving transducers were each attached to a

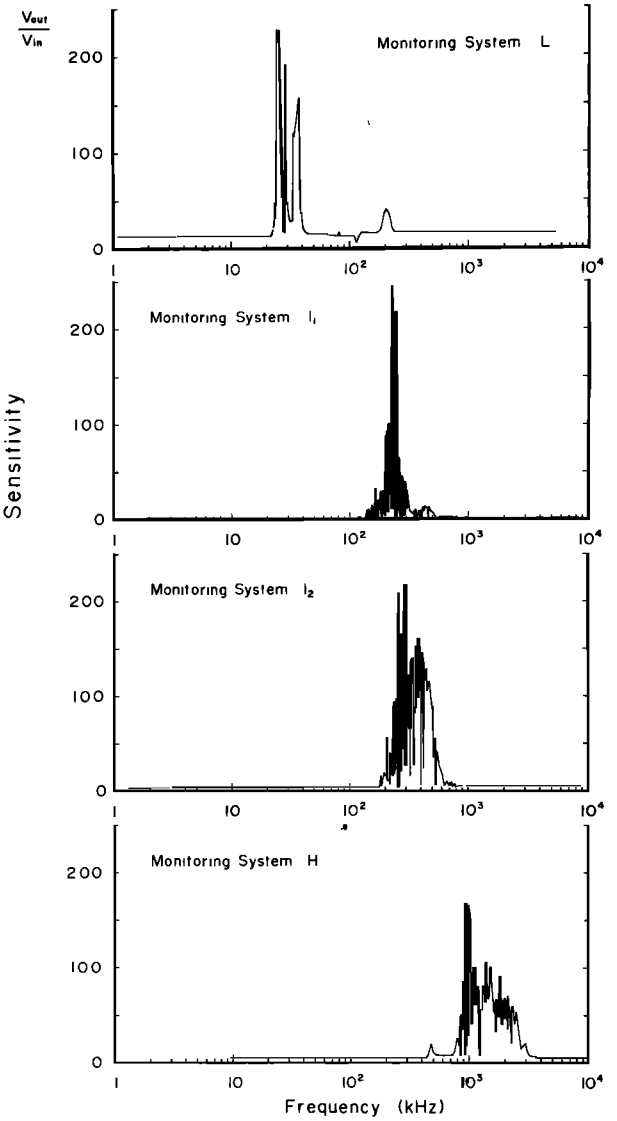

Fig. 1. Four different frequency windows selected and their overall frequency responses.

TABLE 3. Rocks Studied

Rock	Porosity, %	Bulk Density, g/cm^3	P Wave Velocity, km/s	Modal Analysis, %
Shinkomatsu andesite (SAN)	5.3	2.47	4.3	phenocryst 31.6 plagioclase 28.8, augite 1.8, hypersthene 0.5, magnetite 0.5 groundmass 68.4 plagioclase 45.0, pyroxene 19.4, opaque mineral 4.0
Mannari granite (MGR)	0.7	2.62	4.9	quartz 31.1, plagioclase 23.9, K-feldspar 38.5, biotite 4.3, hornblende 0.3, opaque mineral 0.3, chlorite? 1.6

specimen through a brass adapter (about 5 mm thickness), of which one end was finished with great care so as to have the same curvature with the specimen side surface and cemented to the side with epoxy. The specific acoustic impedance ($z_b = 3 \times 10^6$ cgs) of brass is nearly equal to that of the lead zirconate titanate ceramics used ($z_b/z_s=1.09$; where z_s the acoustic impedance of the ceramics), and these acoustic impedances are roughly twice or thrice as large as the acoustic impedance of rock (1.3×10^6 cgs for MGR and 1.1×10^6 cgs for SAN). The two transducers were placed adjacent to each other to minimize the difference in propagation path from emission sources between the two transducers. The flat surfaces of both the transducers and the adapters were carefully polished on plate glass with a fine abrasive. Canada balsam was used as couplant between the polished contact surfaces of both transducers and adapters to achieve good coupling. The transducers for detecting higher-frequency (≳200 kHz) emission events were pressed tightly to the adapters with rubber bands. The transducer for low-frequency (~30 kHz) emission events was screwed to the adapter. Incremental uniaxial compressive load was applied until failure occurred.

EXPERIMENTAL RESULTS

Oscilloscope photographs of some examples of acoustic emission signals observed through the different frequency windows are presented in Figure 2. Shown in Figure 2*a* is an example of emission signals which appeared simultaneously through the frequency windows I_1 and H, indicating that this event has both intermediate (~250 kHz) and high (~1 MHz) frequency wave components. Figure 2*b* shows an example of the events which have dominant high-frequency wave components but few intermediate-frequency components (this event entirely lacks intermediate-frequency components in the initial part of motion), while Figure 2*c* shows an example of the events having dominant intermediate-frequency wave components, but few high-frequency wave components. We classify the emission events monitored through the frequen-

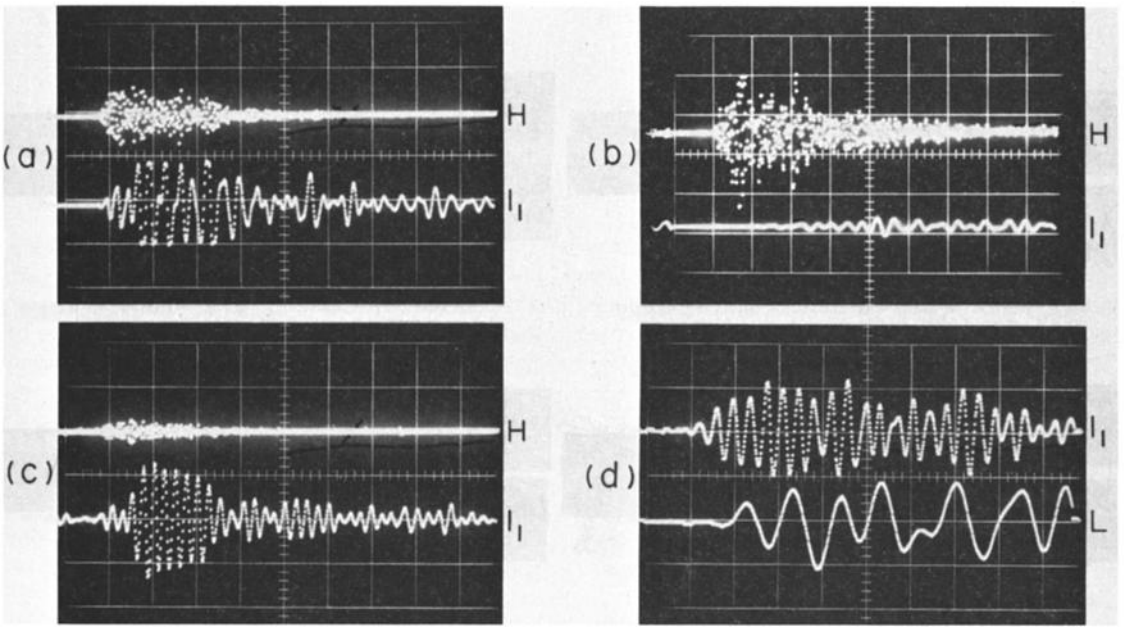

Fig. 2. Oscilloscope photographs of some examples of acoustic emission signals observed. (*a*)–(*c*) Comparison of the emission signals monitored through the high-frequency window H with those monitored simultaneously through the intermediate-frequency window I_1 (time scale, 1 division = 20 μs for Figures 2a and 2b and 1 division = 10 μs for Figure 2*c*). (*d*) Comparison of the emission signals monitored through the frequency window I_1 with those monitored simultaneously through the low-frequency window L (time scale, 1 division = 20 μs).

cy windows I_1 and H into three groups in terms of their relative frequency content. When emission events were monitored through the lower-frequency windows L and I_1, they could also be classified into three groups in terms of the relative frequency content: (1) the emission events having low (~30 kHz) and higher (~250 kHz) frequency components (Figure 2*d*), (2) the events dominated by higher-frequency components, and (3) the events dominated by low-frequency components. These types of events, different in both amplitude and frequency content, were commonly observed even at a nearly constant applied stress. This is one reason why the statistical approach is indispensable when we investigate by comparing the acoustic emission spectra whether there is any systematic change in frequency characteristics of acoustic emissions in rock with an increasing applied stress.

Figure 3*a* shows a plot of a typical example of acoustic emission counts, $n(L)$ and $n(I_2)$, per 10 s against time during the entire process from application of load to failure for incremental, uniaxial compression of Shinkomatsu andesite. The inset shows the site at which the transducers were attached. In this experiment, the two monitoring channels were operated at a gain of 86 dB and a threshold level of 0.5 V(25 μV referred to input). In Figure 3*c* the applied axial stress and the strains (axial, circumferential, and volumetric) are plotted against time for reference. As the axial compressive stress was increased, a flurry of acoustic emission activity occurred at low stresses. This activity died down

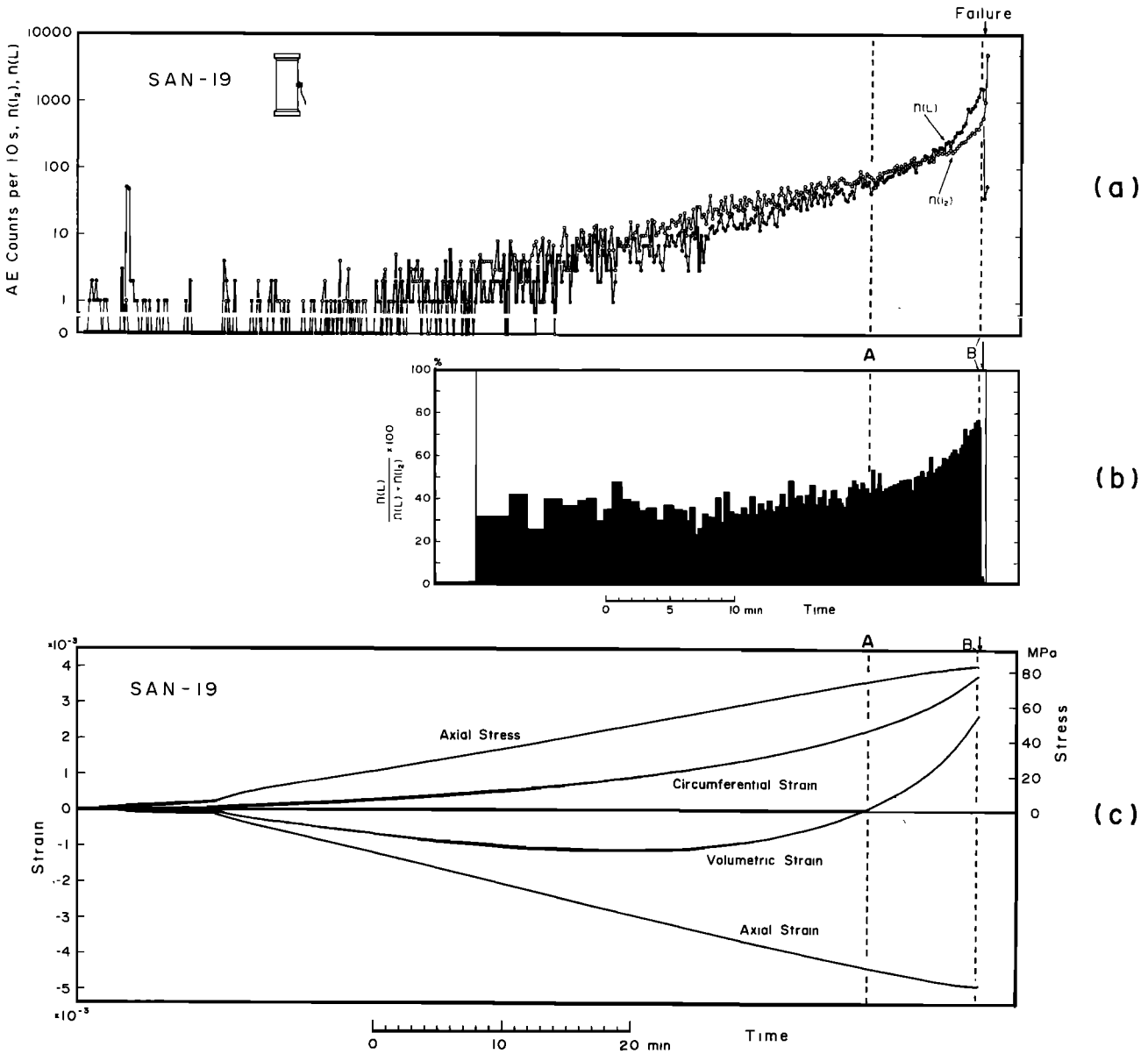

Fig. 3. (*a*) A plot of acoustic emission counts per 10 s, $n(L)$ and $n(I_2)$ monitored through the low-frequency window L and the intermediate-frequency window I_2, respectively, against time during the entire process from application of load to failure. The sample of Shinkomatsu andesite (SAN-19) was incrementally loaded in uniaxial compression. The inset shows the site at which the transducers were attached. (*b*) A plot of $n(L)/(n(L) + n(I_2))$ against time for Shinkomatsu andesite (SAN-19). (*c*) A plot of axial stress and strains (axial, circumferential, and volumetric) against time for SAN-19. The mark A indicates the point in time when $n(L)/(n(L) + n(I_2))$ begins to increase, and the mark B the point in time when a rapid acceleration of higher-frequency acoustic emission rate begins.

very quickly. As the stress was further increased, again acoustic emission activity began to increase, and accelerated rapidly just prior to failure. This pattern has been noticed by numerous earlier authors [e.g., *Scholz,* 1968*a*]. In the present experiments, a typical flurry of acoustic emission activity at low stresses was most consistently observed through the low-frequency window L [cf. *Ohnaka and Mogi,* 1981]. This suggests that most of the activity at low stresses are due to the occurrence of such low-frequency emission events.

We focus attention on frequency characteristics of acoustic emission activity in the region where the activity begins to build up and continues to increase until failure. We find from Figure 3*a* that at first, $n(L)$ and $n(I_2)$ increase exponentially with time, keeping the ratio of $n(L)$ to $n(I_2)$ statistically constant (note that the ordinate of Figure 3*a* is on a logarithmic scale). As rock approaches failure, both $n(L)$ and $n(I_2)$ increase supraexponentially with time, but the rate of increase for $n(L)$ is more rapid than that for $n(I_2)$. Immediately before and during failure there was an extremely rapid rise in higher-frequency emission rate $n(I_2)$. Although it is apparent from Figure 3*a* that the increase rate of $n(L)$ becomes more rapid with time than that of $n(I_2)$, this is seen more clearly in Figure 3*b*, where $[n(L)/(n(L) + n(I_2))] \times 100$ is taken on the ordinate. As stated in the previous section, it is true that the count level itself depends upon the sensitivity and the threshold level set for each channel. But the threshold level and sensitivity were fixed throughout the experiments for each channel. Accordingly, the ratio $n(L)/(n(L) + n(I_2))$ is a useful parameter for checking frequency dependence of the

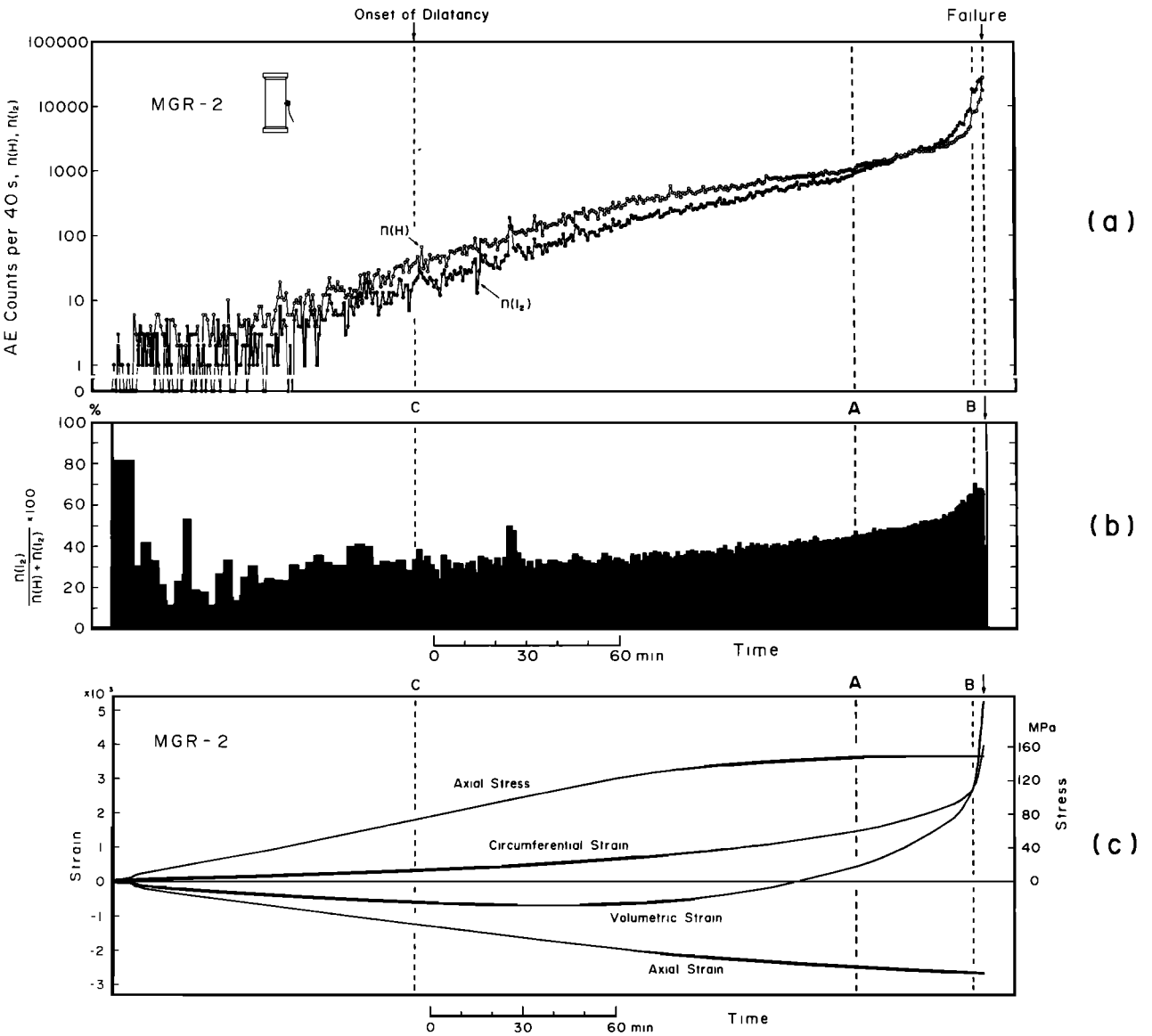

Fig. 4. (*a*) A plot of acoustic emission counts per 40 s, $n(I_2)$ and $n(H)$ monitored through the intermediate-frequency window I_2 and the high-frequency window H, respectively, against time during the entire process from application of load to failure for uniaxial compression of Mannari granite (MGR-2). The inset shows the site at which the transducers were attached. (*b*). A plot of $n(I_2)/(n(I_2) + n(H))$ against time for Mannari granite (MGR-2). (*c*). A plot of axial stress and strains (axial, circumferential, and volumetric) against time for MGR-2. The mark A indicates the point in time when $n(I_2)/(n(I_2) + n(H))$ begins to increase, and the mark B the point in time when a rapid acceleration of higher-frequency acoustic emission rate begins.

emission rate. The change in the ratio defined above may be regarded as a measure of representing the frequency dependence of acoustic emission rate.

Figure 3*b* suggests that the whole process shown in the figure may be tentatively divided into two distinct stages: an early stage where $n(L)/(n(L) + n(I_2))$ is nearly constant, and a later stage where $n(L)/(n(L) + n(I_2))$ increases with time. In this experiment, the transducers were placed at the middle of the specimen, as shown in the inset. Dilatant volume is the largest, and the probability of bond deterioration due to this deformation is the greatest at the middle of the specimen. This may skew the observed frequencies toward the low end. Anisotropic attenuation can be caused by the formation or opening of axial cracks. For these reasons, one may claim that the observed frequency dependence of the emission activity shown in Figure 3 might depend on the transducer sites. Another may question whether the results in Figure 3 are also detected for the emission counts monitored through different pass-band frequency windows. These have been checked, and all the experimental results clearly showed that as the andesite rock approaches failure, the acoustic emission rate generated during the microcracking deformation, monitored through a low-frequency window, increases more rapidly than that monitored simultaneously through a higher-frequency window regardless of the difference in the transducer sites and passband frequencies compared [*Ohnaka and Mogi*, 1981].

Further experiments have been made to examine whether the effect detected for Shinkomatsu andesite, which is porous, is found for nonporous crystalline rock such as granite. In Figure 4*a*, a typical example of acoustic emission counts $n(I_2)$ and $n(H)$ per 40 s are plotted against time during the whole process from application of load to failure for incremental, uniaxial compression of Mannari granite. These counts were sampled every 10 s in the experiment; however, they were summed up every 40 s, and the counts per 40 s were plotted in the figure. The inset shows the site where the transducers were attached. In this experiment, the monitoring channel of H was operated at a gain of 86 dB and a threshold level of 0.3 V (15 μV referred to input), and the channel of I_2 was operated at a gain of 86 dB and a threshold level of 0.5 V (25 μV referred to input). Figure 4*b* shows a plot of the parameter $n(I_2)/(n(I_2) + n(H))$ against time. The two stages defined above are also found in this figure, though a clear boundary is difficult to identify in this case. In Figure 4*c*, the applied axial stress and the strains (axial, circumferential, and volumetric) of the specimen are also plotted against time for reference. In this experiment, the loading rate was held approximately constant for nearly half of the period of time to failure, and then it was gradually decreased to zero. Note that there is a correlation between the slopes of the emission counts-time curve and the applied stress-time curve in the first half of the time to failure. Figure 4 suggests that the emission rate increases exponentially only when the stress rate is constant. We find from Figure 4 that as the failure time approaches the increase in both $n(I_2)$ and $n(H)$ becomes supraexponential with time, as before, and that the increase rate of $n(I_2)$ is more rapid than that of $n(H)$ until a few minutes before failure. Failure occurred shortly after $n(I_2)/(n(I_2) + n(H))$ decreased. These qualitative features are entirely consistent with those found for Shinkomatsu andesite. Similar tests using the frequency windows L and I_2 confirmed qualitatively the observation reported for the windows I_2 and H.

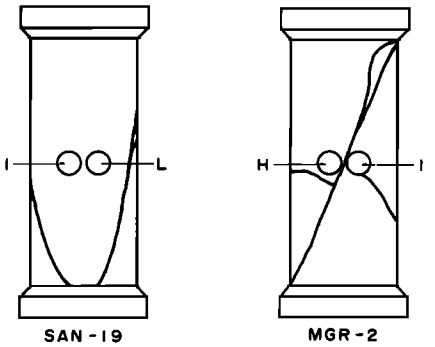

Fig. 5. Relations between the sites to which the transducers were attached and the final macroscopic crack pattern. Transducer sites for monitoring low-frequency (L), intermediate-frequency (I), and high-frequency (H) emission waves are indicated. The thick lines indicate the location of fracture surfaces which were observed when a specimen eventually failed.

Figure 5 illustrates the relation between the sites at which the transducers were attached and the final macroscopic crack pattern for the test specimens of which results are shown in Figures 3 and 4. The thick lines represent the location of fracture surfaces which were observed when the specimens eventually failed.

DISCUSSION

One may claim that the resonance of a loaded cylinder of rock sample and the change of this resonant frequency with deformation might explain the observed frequency dependence of the emission activity. However, this cannot be the case. Let ν be the frequency of sample resonance. Assume that the resonant frequency shifts from ν to $\nu - d\nu$ when rock deforms in the radial direction R to $R + dR$ (R, the radius of a cylindrical specimen). In the present experiments, the radial strain (equal to the circumferential strain) dR/R is less than 5×10^{-3}, and hence $d\nu/\nu < 0.005$. If we assume for instance that I is coincident with ν, then $d\nu < 0.005I = 1.3$ kHz, where $I = 250$ kHz has been assumed. This is negligible change. Even if the increase in $n(I)/(n(I) + n(H))$ is explained by the change of the resonant frequency of the loaded rock sample with deformation, the another fact that $n(L)/(n(L) + n(I))$ increases with deformation cannot be explained by the same assumption.

In the experiment shown in Figure 4, the loading rate was held approximately constant until nearly the half of the whole time from application of load to failure, and then it was gradually decreased to zero. Hence, the applied stress was held nearly constant near failure (Figure 4*c*). Nevertheless, the change in the rate of occurrence of the low band-passed emission events was greater than that of the high band-passed events. Figure 4 gives evidence that the frequency dependence of acoustic emission rate is not necessarily caused by the change in an applied stress level. The frequency dependence could be attributed to the change in microstructure within a deforming rock specimen under compression, as will be discussed in more detail below.

In the preceding section we tentatively divided the region where acoustic emission activity begins to build up and continues to increase until failure, into two stages on the

TABLE 4. Cracking Process to Failure

Stage	Emission Activity	Fracturing Process
I	flurry of acoustic emission activity; $n(l)$ predominant	closure of preexisting cracks at large angles to the compression axis and rupturing of healed portions and asperities
II	low acoustic emission activity	stresses being not high enough for many crackings to occur
III	(exponential) increase in acoustic emission rate; $n(l)/(n(l) + n(h))$ constant	production of new cracks, and opening of cavities at small angles to the compression axis (= onset of dilatancy) in a later phase
IV	supraexponential increase in acoustic emission rate; $n(l)/(n(l) + n(h))$ increase	acceleration of crack-crack interaction
V	rapid acceleration of acoustic emission activity	formation of faults by the rapid coalescence of

$n(l)$, acoustic emission rate monitored through a low-frequency window; $n(h)$, acoustic emission rate monitored through a higher-frequency window.

basis of the result shown in Figure 3 for Shinkomatsu andesite. The deformation process of brittle rock under incremental, uniaxial compression may be commonly divided into the five stages in terms of the acoustic emission rate and the frequency characteristics [*Ohnaka and Mogi,* 1981]. These stages (cf. Table 4) are shown in Figures 6 and 7 compared with complete stress-strain curves typical of Mannari granite and Shinkomatsu andesite. A flurry of acoustic emission activity occurs at low stresses (stage I), as suggested by *Scholz* [1968*a*]. In our experiments, this activity was found to be mostly due to emission events containing low-frequency wave components. One may argue that such a flurry of the activity at very low stresses may be mechanical noises caused by the loading machine. However, great care was taken to eliminate this kind of noise, and the possibility has been checked and found to be rejected. Another possibility is that the activity may be attributed to emission events which may be generated in the epoxy fillets used. This possibility must be considered and may not entirely be rejected. However, the stress-strain curves at low stresses clearly show that compaction occurred in stage I (Figures 6 and 7), and presumably this compaction is due to the closing of preexisting cracks at large angles to the compression axis (note that this compaction is independent of any deformation of the epoxy fillets). Thus, it can be inferred that a flurry of low-frequency acoustic emission activity results from the closing of preexisting long cracks with low aspect ratio at large angles to the compression axis [cf. *Ohnaka and Mogi,* 1981, Figure 8]. In fact, *Sprunt and Brace* [1974] and *Kranz* [1979*a*] revealed the existence of preexisting cracks with such low aspect ratio as 10^{-3}. These low aspect ratio cracks can easily be closed at low stresses, and the closing of preexisting long cracks can generate low-frequency emission waves, as shown below.

The frequency f of an emission signal from an extensional or shear dislocation crack may be estimated from [*Haskell,* 1964; *Ohnaka,* 1976*a*]

$$f \sim 1/[T + (c/v)\,(1 - (v/\beta)\cos\theta)] \qquad (1)$$

where T is the time required for the crack to close, open or shear, c is the crack length, v is the fracture velocity, β is the propagation velocity of the signal, and θ is the angle of the

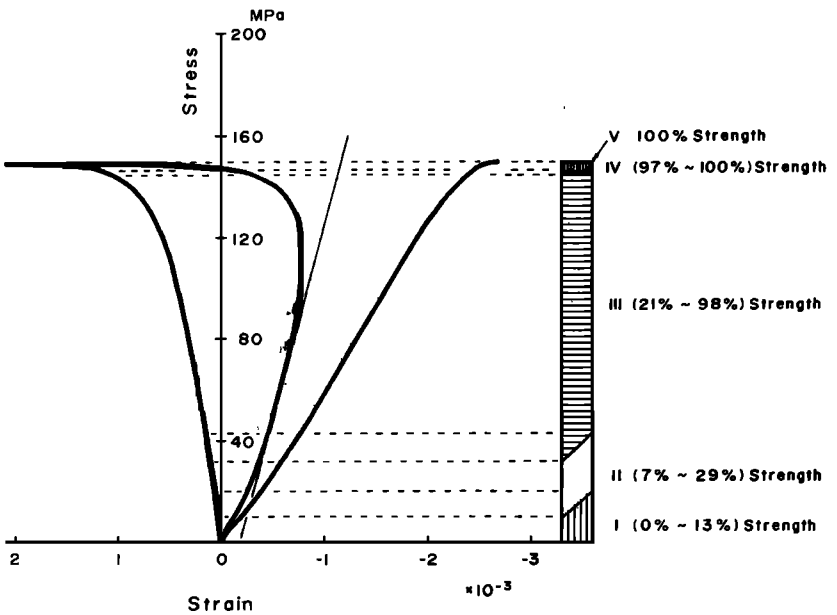

Fig. 6. Stress-strain curves typical of Mannari granite and their relation to the stages I to V.

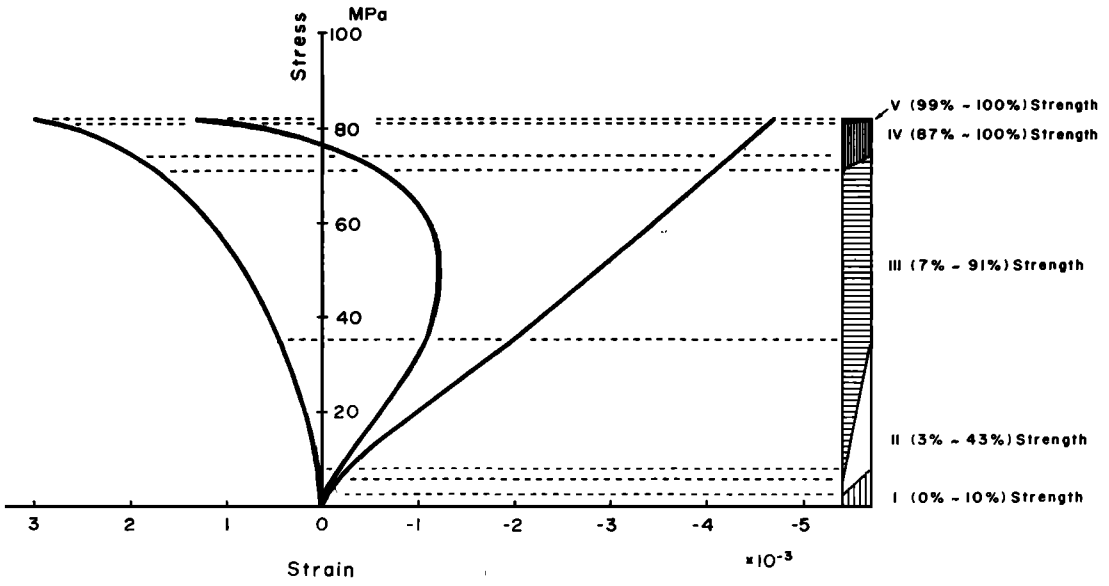

Fig. 7. Stress-strain curves typical of Shinkomatsu andesite and their relation to the stages I to V.

signal propagation to the crack surface. Let θ be $\pi/2$ for simplicity, and (1) is reduced to

$$f \sim 1/[T + (c/v)] \tag{2}$$

T is related to c by

$$T \sim c/v \tag{3}$$

[*Savage*, 1972] or

$$T \sim c/\beta \tag{3'}$$

[*Ohnaka*, 1976*b*]. It is understood from these rough discussions that the closing or opening of existing longer cracks can generate lower-frequency emission signals.

Brace and coworkers [*Sprunt and Brace*, 1974; *Montgomery and Brace*, 1975; *Tapponnier and Brace*, 1976] and *Kranz* [1979*a*] have observed partially healed preexisting cracks in granite with the scanning electron microscope. Rupturing of some of these healed portions and of asperities on preexisting crack surfaces can also occur in this stage, and this will contribute to generating higher-frequency emission waves [see *Ohnaka and Mogi*, 1981, Figure 8.] In the present experiments, the stresses in the stage I were 13% or less of the failure strength (150 MPa) for Mannari granite and 10% or less of the failure strength (82 MPa) for Shinkomatsu andesite.

At higher stresses, the activity dies down to a very low level (stage II). This stage was within the stress range from 7 to 29% of the failure strength for Mannari granite, and from 3 to 43% of the failure strength for Shinkomatsu andesite. This is the stage where almost all of preexisting cracks capable of closing at low stresses have been closed and where local stresses around regions of stress concentration are not high enough for a number of new, stress-induced cracks to occur.

As the stress is further increased gradually, again acoustic emission activity begins to build up and steadily increases (the emission rate increases exponentially when the loading rate is held constant). Both the emission rates $n(l)$ and $n(h)$ monitored through a low-frequency window and a higher-frequency window, respectively, increase with time in statistically the same proportion; that is $n(l)/(n(l) + n(h))$ is nearly constant throughout this stage (stage III). A main feature of this stage would be that new, stress-induced cracks are produced successively. In the present experiments, stage III was within the stress range from 21 to 98% of the failure strength for Mannari granite and from 7 to 91% of the strength for Shinkomatsu andesite. *Scholz* [1968*a*] reported that the beginning of a sequence of acoustic emission activity corresponds to the onset of dilatancy defined as the beginning of the nonlinear part of the axial stress–volumetric strain curve above about half the failure strength. In the present experiments, however, the beginning of stage III was not concurrent with the onset of dilatancy defined above. The sequence of acoustic emission activity in practice began at low stresses where appreciable dilatancy did not appear to begin. This will be discussed in more detail later.

As the failure time approaches, both $n(l)$ and $n(h)$ increase supraexponentially with time, and the increase rate of $n(l)$ becomes more rapid than that of $n(h)$ until immediately before failure (stage IV: from the point of time marked A to the point of time marked B in Figures 3 and 4). In other words, this stage is characterized by an increase in $n(l)/(n(l) + n(h))$ with time or by a higher level of $n(l)/(n(l) + n(h))$. Appreciable dilatancy always began to occur prior to the beginning of this stage. In the present experiments, stage IV was within the stress range from 97 to 100% of the failure strength for Mannari granite and from 87 to 100% of the strength for Shinkomatsu andesite. Stage IV is important in understanding the microcracking process leading up to failure, and hence this stage discussed in detail separately below.

Stage V (final stage: from the point of time marked B to failure time in Figures 3 and 4) is characterized by a very rapid acceleration of higher-frequency emission rate immediately before and during failure. *Sondergeld et al.* [1980] have reported that the high-frequency content of an acoustic emission event increases just prior to rock failure. This is consistent with present results. Failure occurs immediately after $n(l)/(n(l) + n(h))$ decreases. The stress in this stage was as high as the failure strength for both rocks studied.

One interesting feature in these stages would be that the increase rate of the acoustic emission counted through a lower-frequency window becomes more rapid with time in stage IV. This is not necessarily due to the change in an applied stress level itself, as described above, but due to the change in microstructure within a deforming rock specimen. As suggested elsewhere [*Ohnaka and Mogi*, 1981], there are two possible explanations for this.

1. As an applied stress increases, microfractures will occur and the resulting microcracks will further grow to some extent and develop (or coalesce) in the course of deformation. Opening or shearing of these existing cracks into larger sizes tends to generate emission waves containing lower-frequency components, as shown above. The number of these larger cracks is likely to increase greatly with time as rock approaches failure. As a result, lower-frequency emission waves will be generated more in this stage.

2. As an applied stress increases, microcracks will increase in number and will be distributed within a rock specimen during the deformation, causing a dilatant region within it. The development of such a dilatant region has the effect of attenuating emission waves. In a stage where dilatancy is pronounced and widely developed, the emission events with low-frequency wave components become more highly detectable. Higher-frequency wave components are more highly attenuated as they propagate away from the source. *Holcomb* [1978] and *Nishizawa et al.* [1980] have shown that as rock approaches failure, the attenuation increases most strongly at higher frequencies. Thus, we would expect to see only the lower frequencies.

Both explanations given above may be partly responsible for the observed frequency dependence; however, it is difficult to determine in quantitative terms from the present experiments to what extent each is responsible. Recently, *Tapponnier and Brace* [1976] and *Kranz* [1979*a*, *b*], using the scanning electron microscope, have examined how cracks grow, develop, and interact in rock under compression and suggested that crack interaction and coalescence become more important before macrofracture than the formation of individual, new cracks. A similar idea (critical crack density) has been offered by *Scholz* [1968*c*], *Cruden* [1974], and *Mjachkin et al.* [1975] to explain the initiation of macrofracture. These support the above presumption that the number of larger cracks increases as rock approaches failure. We suggest that the onset of stage IV marked A in Figures 3 and 4 may correspond to the point when crack interaction and coalescence begin to dominate.

In the statistical analysis of acoustic emission during the microcracking process of rock, a log-log plot of the cumulative number of events versus the maximum trace amplitude is conventionally employed to display the amplitude distribution data [*Mogi*, 1962*a*, *b*, 1981; *Scholz*, 1968*d*]. In this plot, the curve is a monotonically decreasing function of the amplitude and generally can be expressed by one or more straight-line segments. The slope of the curve which is a characteristic of the amplitude distribution is called '*m* value' or '*b* value' ($b = m - 1$). It has been reported that the *m* value decreases as rock approaches failure [e.g., *Scholz*, 1968*d*; *Mogi*, 1981]. In particular, *Mogi* [1981] found the decrease in *m* value before failure under an applied constant stress. This means that the number of emission events with larger amplitude increases more in relative terms as rock approaches failure. This effect can be explained reasonably if the source dimension (crack size) and/or the stress drop of individual emission events become larger in statistical terms as rock approaches failure. If the effect means that the number of crack resulting in larger sizes increases more in relative terms as rock approaches failure, then the decrease in *m* value could be consistent with the observed frequency dependence of acoustic emission rate in stage IV. Larger cracks tend to generate emission waves both having larger amplitudes and containing lower-frequency components. We conclude that both the decrease in *m* value [e.g., *Scholz*, 1968*d*; *Mogi*, 1981] and the frequency dependence of acoustic emission rate found here are different manifestations of an aspect of the microcracking process leading to failure of brittle rock.

A greater number of higher-frequency emission events observed in stage V may be thought to be those originating around the transducers as a result of local stress concentrations near the adapters during the process of forming final faults by the rapid coalescence of larger cracks. Figure 5 in this paper and Figure 9 in the previous paper [*Ohnaka and Mogi*, 1981] suggest that the transducer sites can be sources of stress concentration.

A summary of the microcracking process leading up to failure for the rocks tested is presented in Table 3, where only a typical, dominant mode characterizing each stage is listed. For example, new independent cracking and interaction between preexisting cracks and new cracks will, in practice, occur in both stages III and IV. However, the present experimental results support the idea, presented by earlier authors [e.g., *Kranz*, 1979*a*], that crack-crack interaction (or crack coalescence) is becoming more important as the failure time approaches.

As pointed out above, the beginning of a sequence of acoustic emission activity does not necessarily correspond to the onset of dilatancy which is defined by *Brace et al.* [1966] as the beginning of the nonlinear part of the axial stress-volumetric strain curve above about half the failure strength (see Figure 6). In general, if the sensitivity of the monitoring system is high, the beginning of a sequence of acoustic emission activity will be observed at lower stresses. In fact, our high sensitivity and low noise counting system (Table 1) made it possible to detect a sequence of emission activity below the onset of dilatancy (Figure 4 or 6 in this paper and see also Figure 8 of *Ohnaka and Mogi* [1981]). Note in these figures that stage III begins prior to the onset of dilatancy. Other researchers [e.g., *Kurita and Fujii*, 1979] have also observed the acoustic emission activity in rock prior to the onset of dilatancy.

As stated above, a sequence of acoustic emission activity begins prior to the onset of the appreciable (measurable) dilatancy; that is, acoustic emissions are generated in the 'linear part' of the stress-strain curve (Figure 4 or 6). These observations suggest that even a low porosity rock such as granite cannot be purely elastic in the 'linear part' of the stress-strain curve because the generation of acoustic emission involves locally inelastic processes [*Brodsky and Spetzler*, 1979]. This 'linear part' of the stress-strain curve may be called pseudoelastic, and the 'linear part' of the stress-strain curve is defined as the region in which each cracking contributes only a negligibly small increment to the volumetric strain. *Paterson* [1978] suggests that there may be no truly linear portion of the stress-strain curve in rocks of appreciable porosity or previous microcracking history.

The onset of dilatancy defined by *Brace et al.* [1966] corresponds to a phase where existing cracks at small angles to the compression axis begin to open [*Tapponnier and Brace*, 1976], and this does not necessarily correspond to the beginning of a sequence of acoustic emission activity. These arguments appear very plausible because rock is made up of several kinds of minerals (different in grain size, shape, and compositon) and contains microcracks and pores, and hence rock involves innumerable regions of potential stress concentration around such grain boundaries and tips of microcracks and pores. Small cracks which occur at lower applied stresses presumably do not contribute an appreciable increase in cavity volume.

For high porosity rocks such as Shinkomatsu andesite containing high aspect ratio cavities, the closing of pores, the resulting compaction [e.g., *Bridgman*, 1918], and the induced microcracks can occur continuously during the deformation process from application of load to failure. As a result the effect of compaction and dilatancy is difficult to separate [*Paterson*, 1978]. In fact, *Brace* [1978] has pointed out that both compaction and dilatancy occur at the same time when rocks have more than about 5% porosity. For this reason, the actual onset of dilatancy is more difficult to identify for Shinkomatsu andesite.

We have found in this series of experiments that the acoustic emission rate monitored through a low-frequency window increases more rapidly than that monitored simultaneously through a high-frequency window as rock approaches failure under compression. This effect may be utilized in understanding structural instability of a region where rockbursts or earthquakes can potentially occur. If a sizable microseismic population is observed through sensors placed in the region, then a potential exists for forecasting major earthquakes.

Acknowledgments. We would like to express our sincere thanks to the reviewers of JGR for critical review of the manuscript.

REFERENCES

Brace, W. F., Volume changes during fracture and frictional sliding: A review, *Pure Appl. Geophys., 116,* 603–614, 1978.

Brace, W. F., and A. S. Orange, Electrical resistivity changes in saturated rocks during fracture and frictional sliding, *J. Geophys. Res., 73,* 1433–1445, 1968.

Brace, W. F., B. W. Paulding, Jr., and C. Scholz, Dilatancy in the fracture of crystalline rocks, *J. Geophys. Res., 71,* 3939–3953, 1966.

Bridgman, P. W., The failure of cavities in crystals and rocks under pressure, *Am. J. Sci., 45,* 243–268, 1918.

Brodsky, N., and H. Spetzler, Time dependent deformation of a basalt at low differential stress, *Proc. Lunar Planet. Sci. Conf., 10th,* 2155–2163, 1979.

Byerlee, J. D., and D. Lockner, Acoustic emission during fluid injection into rock, in *Proceedings of the 1st Conference on Acoustic Emission/Microseismic Activity in Geologic Structures and Materials,* edited by H. R. Hardy, Jr. and F. W. Leighton, pp. 87–98, 1977.

Chugh, Y. P., H. R. Hardy, Jr., and R. Stefanko, An investigation of the frequency spectra of microseismic activity in rock under tension, in *Proceedings of the 10th Rock Mechanics Symposium, (Austin, 1968),* edited by K. E. Gray, pp. 73–113, AIME, New York, 1972.

Cruden, D. M., The static fatigue of brittle rock under uniaxial compression, *Int. J. Rock Mech. Min. Sci. Geomech. Abstr., 11,* 67–73, 1974.

Furukawa, E., *Vibration and Shock Measurements* (in Japanese), 375 pp., Seibundoshinkosha, Tokyo, 1966.

Hardy, H. R., Jr., Application of acoustic emission techniques to rock mechanics research, *ASTM Spec. Tech. Publ., STP505,* 41–83, 1972.

Haskell, N. A., Total energy and energy spectral density of elastic wave radiation from propagating faults, *Bull. Seismol. Soc. Am., 54,* 1811–1841, 1964.

Holcomb, D. J., A theoretical and experimental investigation of dilatancy: An aspect of nonlinear behavior in rock, Ph. D. thesis, Univ. of Colo., Boulder, 1978.

Kanagawa, T., M. Hayashi, and H. Nakasa, Estimation of spacial geo-stress components in rock samples using the Kaiser effect of acoustic emission (in Japanese), *Proc. Jpn. Soc. Civ. Eng., 258,* 63–75, 1977.

Kranz, R. L., Crack growth and development during creep of Barre granite, *Int. J. Rock Mech. Min. Sci. Geomech. Abstr., 16,* 23–35, 1979*a*.

Kranz, R. L., Crack-crack and crack-pore interactions in stressed granite, *Int. J. Rock Mech. Min. Sci. Geomech. Abstr., 16,* 37–47, 1979*b*.

Kurita, K., and N. Fujii, Stress memory of crystalline rocks in acoustic emission, *Geophys. Res. Lett., 6,* 9–12, 1979.

Kusunose, K., K. Yamamoto, and T. Hirasawa, Source process of microfracture in granite with reference to earthquake prediction, *Sci. Rep. Tohoku Univ. Ser. 5, 26,* 111–121, 1980.

Lockner, D., and J. Byerlee, Acoustic emission and fault formation in rocks, in *Proceedings of the 1st Conference on Acoustic Emission/Microseismic Activity in Geologic Structures and Materials,* edited by H. R. Hardy, Jr. and F. W. Leighton, pp. 99–107, 1977*a*.

Lockner, D., and J. D. Byerlee, Hydrofacture in Weber sandstone at high confining pressure and differential stress, *J. Geophys. Res., 82,* 2018–2026, 1977*b*.

Matsushima, S., Variation of the elastic wave velocity of rocks in the process of deformation and fracture under high pressure, *Bull. Disaster Prev. Res. Inst., Kyoto Univ., 32,* 1–8, 1960.

Mjachkin, V. I., W. F. Brace, G. A. Sobolev, and J. H. Dieterich, Two models for earthquake forerunners, *Pure Appl. Geophys., 113,* 169–181, 1975.

Mogi, K., Study of elastic shocks caused by the fracture of heterogeneous materials and its relations to earthquake phenomena, *Bull. Earthquake Res. Inst., Tokyo Univ., 40,* 125–173, 1962*a*.

Mogi, K., Magnitude-frequency relation for elastic shocks accompanying fractures of various materials and some related problems in earthquakes, 2, *Bull. Earthquake Res. Inst., Tokyo Univ., 40,* 831–853, 1962*b*.

Mogi, K., Some precise measurements of fracture strength of rocks under uniform compressive stress, *Felsmech. Ingenieurgeol., 4,* 41–55, 1966.

Mogi, K., Source locations of elastic shocks in the fracturing process in rocks, 1, *Bull. Earthquake Res. Inst., Tokyo Univ., 46,* 1103–1125, 1968.

Mogi, K., Earthquake prediction program in Japan, in *Earthquake Prediction: An International Review, Maurice Ewing Ser.,* vol. 4, edited by D. W. Simpson and P. G. Richards, pp. 635–666, AGU, Washington, D. C., 1981.

Montgomery, C. W., and W. F. Brace, Micropores in plagioclase, *Contrib. Mineral. Petrol., 52,* 17–28, 1975.

Nishizawa, O., H. Ito, and T. Ishido, Elastic wave spectra and cracks in rock, II (in Japanese), *Program. Abstr. Seismol. Soc. Jpn. 2,* 133, 1980.

Nishizawa, O., K. Kusunose, and K. Onai, A study of space-time distribution of AE hypocenters in a rock sample under uniaxial compression, *Bull. Geol. Surv. Jpn., 32,* 473–486, 1981.

Nur, A., and G. Simmons, Stress-induced velocity anisotropy in rock: an experimental study, *J. Geophys. Res., 74,* 6667–6674, 1969.

Obert, L., and W. I. Duvall, Use of subaudible noise for prediction of rock bursts, part II, *Rep. Invest. U.S. Bur. Mines, 3654,* 1942.

Ohnaka, M., A physical basis for earthquakes based on the elastic rebound model, *Bull. Seismol. Soc. Am., 66,* 433–451, 1976*a*.

Ohnaka, M., Rise time of source time function and average slip velocity (in Japanese), *Zisin, 29,* 318–320, 1976*b*.

Ohnaka, M., and K. Mogi, Frequency dependence of acoustic emission activity in rocks under incremental, uniaxial compression, *Bull. Earthquake Res. Inst., Tokyo Univ., 56,* 67–89, 1981.

Paterson, M. S., *Experimental Rock Deformation—The Brittle Field,* 254 pp., Springer-Verlag, New York, 1978.

Savage, J. C., Relation of corner frequency to fault dimensions, *J. Geophys. Res.*, *77*, 3788–3795, 1972.

Scholz, C. H., Microfracturing and the inelastic deformation of rock in compression, *J. Geophys. Res.*, *73*, 1417–1432, 1968*a*.

Scholz, C. H., Experimental study of the fracturing process in brittle rock, *J. Geophys. Res.*, *73*, 1447–1453, 1968*b*.

Scholz, C. H., Mechanism of creep in brittle rock, *J. Geophys. Res.*, *73*, 3295–3302, 1968*c*.

Scholz, C. H., The frequency-magnitude relation of microfracturing in rock and its relation to earthquakes, *Bull. Seismol. Soc. Am.*, *58*, 399–415, 1968*d*.

Shamina, O. G., Elastic pulses in the fracture of rock samples (in Russian), *Izv. Akad. Nauk SSSR Ser. Geofiz.*, *5*, 513–518, 1956.

Sondergeld, C. H., and L. H. Estey, Acoustic emission study of microfracturing during the cyclic loading of Westerly granite, *J. Geophys. Res.*, *86*, 2915–2924, 1981.

Sondergeld, C. H., I. C. Getting, H. A. Spetzler, and G. Sobolev, Observations of velocity changes during the deformation of pyrophyllite, *Pure Appl. Geophys.*, *118*, 975–989, 1980.

Sprunt, E. S., and W. F. Brace, Direct observation of microcavities in crystalline rocks, *Int. J. Rock Mech. Min. Sci. Geomech. Abstr.*, *11*, 139–150, 1974.

Tapponnier, P., and W. F. Brace, Development of stress-induced microcracks in Westerly granite, *Int. J. Rock Mech. Min. Sci. Geomech. Abstr.*, *13*, 103–112, 1976.

(Received May 26, 1981;
revised January 15, 1982;
accepted January 22, 1982.)